A PROBABILISTIC APPROACH TO REACTION COORDINATE AND RATE CONSTANT MODELING APPLIED TO EPOXIDE RING-OPENING REACTIONS

by

DALE GREEN

B.S., Texas Tech University, 2001

A REPORT

submitted in partial fulfillment of the requirements for the degree

MASTER OF SCIENCE

Department of Chemical Engineering
College of Engineering

KANSAS STATE UNIVERSITY
Manhattan, Kansas

2012

Approved by:

Major Professor
Dr. Keith Hohn

Abstract

The study will utilize a probabilistic reaction modeling method for ring-opening reactions of epoxide. In particular, to elucidate the reaction mechanism by the methods presented, focus will be placed on the nucleophillic attack of ethylene oxide by ammonia and its anion. This focus was chosen because of the potential to gain significant advantage in computational intensity required to model the epoxy-amino macromolecular curing reactions and resulting thermochemical and physical properties of the cured resin.

The method employed utilizes the combinatorial probability that

1. Two molecules will approach a transition state with sufficient energy to drive reaction
2. Any reaction will occur for a given penetration into the potential energy surface. The concept of a transition state is relaxed to allow a dynamic probability that any reaction will proceed given a position on the intrinsic reaction coordinate (IRC) rather than searching for a specific transition state of theoretical reaction probability.
3. The reaction that occurs yields a desired stable or semi-stable molecular complex

This study will focus on identifying possible stable and semi-stable products and corresponding rate constants. The technique developed here is novel in that it provides an unsupervised method to identify all structures corresponding to minima on the potential energy surface. The technique provides a pragmatic and efficient approach to sample a molecular system for different reaction mechanisms and provides a relative energy requirement to achieve these mechanisms with no presupposition of the mechanism, product, or transition state. It is possible from this data to derive rate constants for a reacting system, however, the rate constant derived for the EO/NH2 molecular system yielded significantly understated reaction probabilities and therefore rate constants.

Table of Contents

List of Figures

List of Tables

Acknowledgments

I would like to thank my wife and best friend, Tammy Green, for her unwavering love and support. She has heard more about this effort than anyone, and for that, I really should apologize. I would like also to thank my daughter, for giving me hope and keeping me going. I would like also to thank my parents for always being there for me.

In addition, I would like to thank Dr. Keith Hohn who was kind enough to guide me through this process and offer a knowledgeable ear. Finally, I would like to thank the Division of Continuing Education of Kansas State University. This is really a fantastic and well organized program. It is certainly nothing like my first degree on campus, but well worth the effort.

Chapter 1. Epoxide Ring Opening Chemistry

Two types of reaction mechanisms are responsible for the epoxy curing process: polyaddition reactions and homopolymerization. These are discussed in detail relevant to their respective roles in the curing process by Petrie (1). The former occurs either by cationic or anionic means and involves the addition of a curing agent or hardener to the oxirane as shown in Figure 1-1. This reaction, which is the focus of this study, allows for cross-linking of the resin at lower barrier energies than its counterpart and therefore will dominate the beginning of the cure until stoichiometric ratios become unfavorable.

Figure 0-1. Polyaddition Reaction Sequence (1)

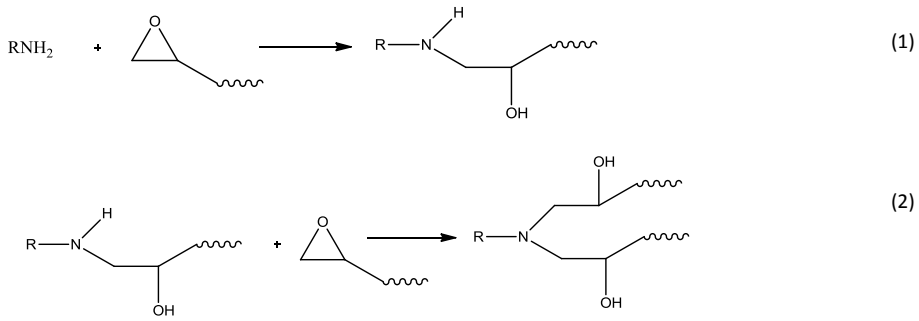

Ring opening reactions of an epoxide ring proceed by Sn2 mechanism as shown below. The traditional interpretation of this reaction occurs by an underside ring attack, or anti configuration. This interpretation exists because this is the classical mechanism for Sn2 reactions and also because the resulting transition state to the zwitterion complex, while not stabilized by the nucleophillic hydrogen in ammonia, has been shown to possess a lower energy barrier (39.4 vs. 54.1 kcal/mol) than that of the top side attack, or syn, configuration when the reaction takes place in vacuo (2).

Figure 0-2. Nucleophillic Addition to Oxirane by Sn2 Mechanism

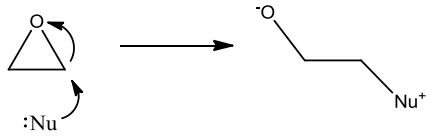

The present work will analyze this mechanism in detail via Monte Carlo simulation across the entire potential energy surface and will show that while minimums do exist in the potential energy surface, the combination of available area for interaction coupled with competing reactions may negate the favorable energy benefit from the anti transition state. Because of the complexity of the surface, many independent and fully converged transition states may be found at comparable levels of theory to the above work, however, the full probability that these transition states are utilized by actual interacting molecules is a function of the probability that paths yielding lower energy transition states are equally accessible to their higher energy counterparts. Stated more plainly, transition state theory inherently assumes equilibrium based on all relative energies and does not consider effects such orientation requirements during molecular collision that would be increasingly important with increasing complexity and size of the system. For implementation of traditional TST, these effects would generally be accounted for in the transmission coefficient. The present work, however, will attempt to map explicitly these probabilities.

In figures 1-3 and 1-4, the Walsh diagrams for each of the reacting systems are constructed. These are useful to understand qualitatively the interactions that take place during reaction.

Figure 0-3. Ethylene Oxide-NH2 Walsh Diagram (Anti Configuration)

- *All structures optimized and fully converged to 0.001 kcal/mol at 6-31G* level*
- *Orbital energies calculated at MP2/6-31G**

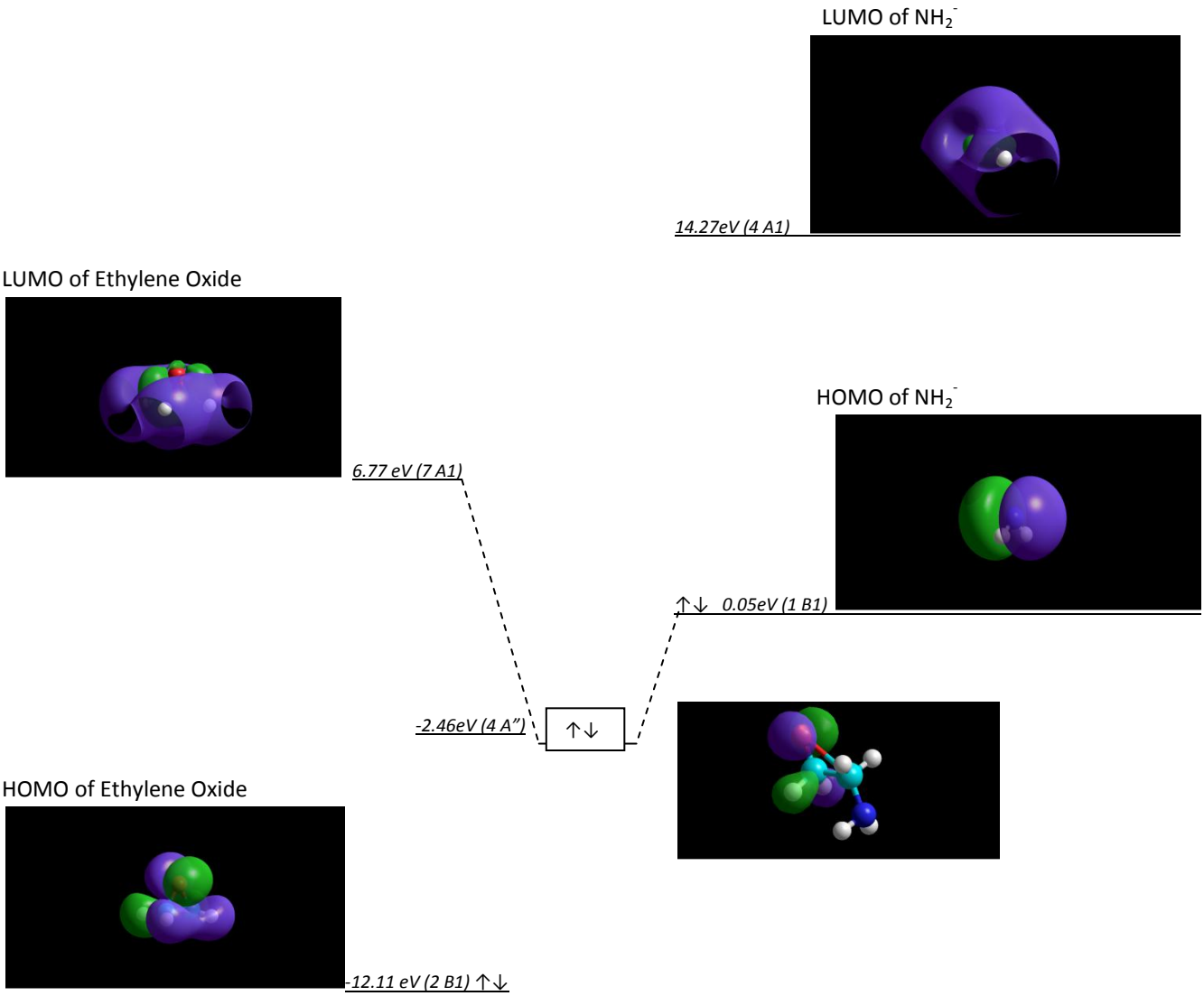

Figure 0-4. Ethylene Oxide-NH3 Walsh Diagram

- *All structures optimized and fully converged to 0.001 kcal/mol at 6-31G* level*
- *Orbital energies calculated at MP2/6-31G**

LUMO of Ethylene Oxide

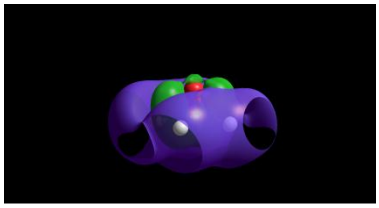

6.77 eV (7 A1)

LUMO of NH_3

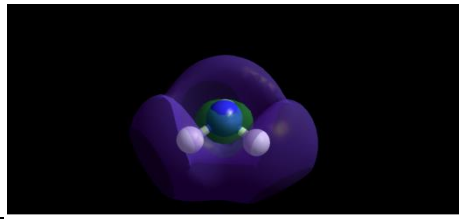

6.06eV (4 A1)

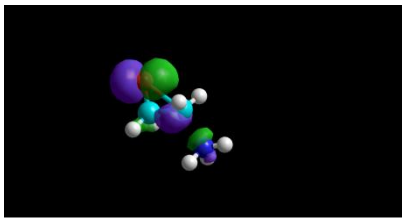

-7.82eV (4 A") ↑↓

HOMO of Ethylene Oxide

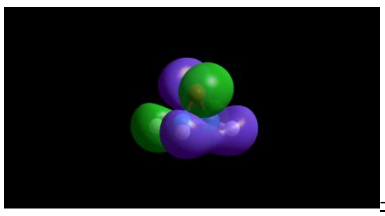

-12.11 eV (2 B1) ↑↓

HOMO of NH_3

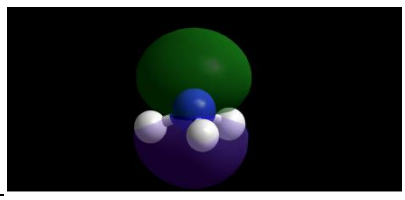

↑↓ *-11.42eV (3 A1)*

Chapter 2. Overview of PM3 Semi-Empirical Method

Purpose

While the methods employed here do not require the computational energy that would be required for a complete search for every possible transition state, use of higher level theory to achieve accuracy across the procedure is beyond the capabilities of the utilized hardware platform. The computational cost of semi-empirical methods make them desirable, however, they have historically performed very poorly as molecules move away from equilibrium structures. It is therefore necessary to estimate the accuracy of this lower level of theory and therefore qualify the application to model non-equilibrium structures along the epoxide-amino reaction coordinate.

PM3 method was chosen as a compromise between accuracy for estimation of key thermochemical data for the elements involved and speed of implementation. All calculations throughout this study were performed using HyperChem™ (3).

PM3 Background

The PM3 semi-empirical method was developed by Stewart through a novel regression of parameters against the modified neglect of diatomic orbital (MNDO) method (4). The original implementation of PM3 was regressed for 12 elements (H, C, N, O, F, Al, Si, P, S, Cl, Br, I) utilizing 18 parameters. It is such named because it is the 3rd major regression performed on the MNDO method: Parametric Method 3. Unlike AM1, the second parameterization of MNDO which utilized both intuition and statistical parameter fitting, PM3 was fully parameterized by unsupervised statistical methods. As a result, the method varies significantly with AM1 with respect to specific parameters.

The application of PM3 to reaction coordinates has historically led to errant results. Malwitz (5) showed that while the PM3 method systematically led to overestimated barrier heights, the results were consistent in the offset and therefore allowed a calibration of $\Delta G^{\ddagger}$ for isocyanate reactions. A recent application by Pu and Truhlar (6) of PM3 to the hydrogen abstraction of methanol by a hydrogen atom reiterates the issues that lie within the method to predict heats of formation of transition states. This study is of particular interest because the results show the tendency of PM3 to severely underestimate barrier height of hydrogen abstraction from a stable molecule by an anion. There are references also to a known error in the charges calculated for nitrogen atoms in PM3 which have been since been corrected in RM1, a re-parameterization of AM1, however, no documentation exists in the literature depicting or addressing these errors.

Figure 2-1 shows the fit of PM3 predicted heats of formation to experimental (or predicted via high level *ab initio* methods) from a published dataset of ~3000 compounds (7). Figure 2-2 is an analysis performed after outliers are removed from both the AM1 and PM3 data that prevent a normal distribution of the data (~10% of the 3000 compound dataset) and shows performance of PM3 is superior to AM1 for these 3000 compounds.

Figure 2-1. PM3 Prediction of Heats of Formation for 3000 compounds

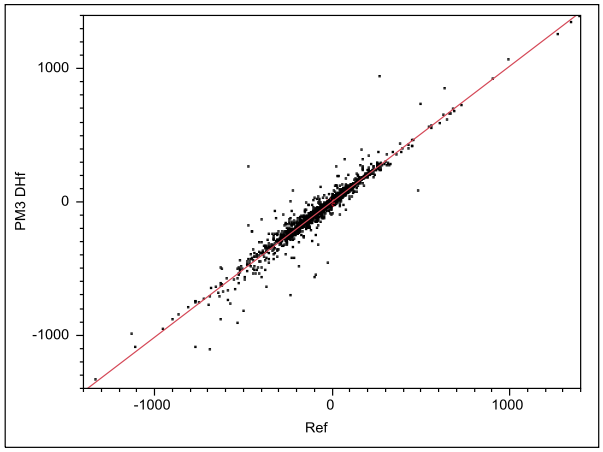

Summary of Fit	
RSquare	0.933414
RSquare Adj	0.933392
Root Mean Square Error	43.64967
Mean of Response	-52.4573
Observations (or Sum Wgts)	3032

Figure 2-2. Comparison of PM3 to AM1 for Errors in Prediction of Heats of Formation

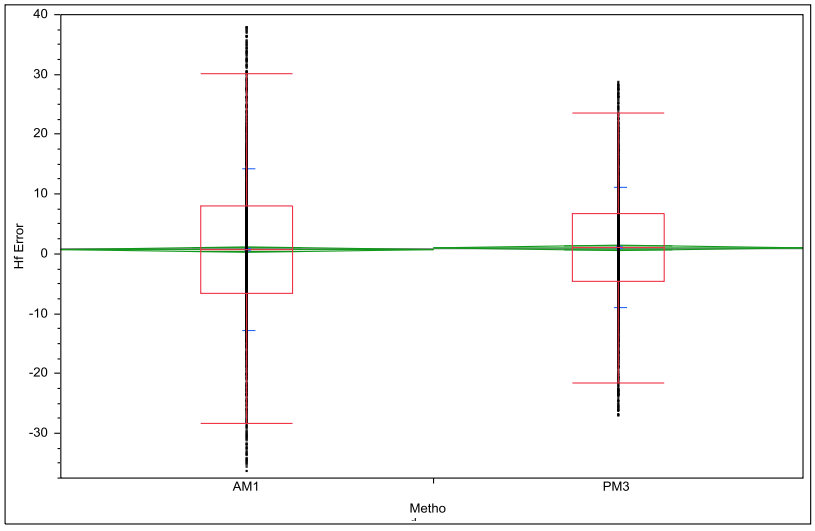

PM3 Accuracy - Comparison of Transition State Structures

The ability of the PM3 to accurately predict transition state barrier heights and thermochemical properties will be first evaluated using a comparison of transition state structures derived at a higher level (i.e. *ab initio)* of theory with PM3 derived structures. Where possible, literature values were used.

For reference, the total energy for each reactant is tabulated in Table 2-3.

Table 2-3. Reactant Total Energies

Method	EO Total Energy (kcal/mol)	NH3 Total Energy (kcal/mol)	NH2 Total Energy (kcal/mol)
PM3	-13626.5	-4811.57	-4416.62
AM1	-14531.9	-5732.77	-5358.09
RM1	-14350.1	-5833.42	-5442.58
Ab Initio *-Geometry by RHF-6-31G** *- Energy calculated by RHF-6-31G**	-95925.7	-35256.2	-34811.8
Ab Initio *- Energy calculated by MP2/RHF-6-31G**	-96205.9	-35364.5	-34920.7

EO-NH_3 Anti Transition State

The transition state for anti configuration of the EO / NH3 reacting system was derived and fully converged utilizing PM3, AM1, RM1, and RHF-6-31G* methods. For this transition state, literature values for both geometry and barrier height were reported by Holubka (2). Comparison across the calculated and reported results allows for a benchmark of the methods and conclusions within this study against those presented in that work.

There was an offset of ~3 kcal/mol between the reported values for the transition state in literature and the values calculated here utilizing a slightly lower level of theory (MP2 vs. MP4SDTQ). PM3 provided an accurate estimate of the barrier height and TS geometry calculated at the MP2 level of theory and outperformed AM1 and RM1.

Based on this assessment, little or no correction must be made to apply PM3 to the model for this transition state.

Figure 2-4. EO/NH3 Anti transition state derived from PM3 level of theory

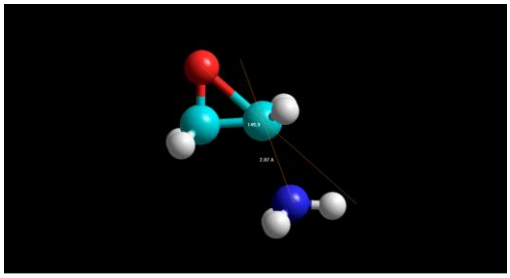

Table 2-5. Comparison of method performance for prediction of EO/NH3 barrier heights

Transition State	Method	O1-C1-N1 Angle (deg)	C1-N1 Bond Length (A)	Total Potential Energy (kcal/mol)	Activation Barrier (kcal/mol)	Notes on Generation
Anti	PM3	153.3	1.846	-18396	42.37	- Placed N1 at 1.6 A off C1 - MM Optimization for fixed EO molecule - PM3 Optimization for 6 cycles - Eigenvector transition state search
Anti	AM1	156.2	1.871	-20220	44.37	
Anti	RM1	150.1	1.961	-20150	33.82	
Anti	Ab Initio *-Geometry by RHF-6-31G** *- Energy calculated by RHF-6-31G**	154.9	1.821	-131132	49.9	- PM3 transition state optimization - Eigenvector transition state search
Anti	Ab Initio *- Energy calculated by MP2/RHF-6-31G**			-131528	42.4	
Anti	Ab Initio *-Geometry optimization by HF-6-31G** *- Energy calculated by MP4SDTQ/6-31G**	154.9	1.822		39.5	Literature value

EO-NH_2 Anti Transition State

The exercise above was repeated replacing the ammonia molecule with its deprotonated anion. Results are depicted in Table 2-6. Unlike the EO-ammonia system, there was consistent and significant deviation between levels of theory evaluated here. There appear to be two causes associated with this deviation:

1. Overestimation of hydrogen bond strength between the oxirane protons and lone pair on NH_2.
2. Elevated state(s) along the IRC that include the transition state

Table 2-6. Comparison of method performance for prediction of EO/NH2 barrier heights

Transition State	Method	O1-C1-N1 Angle (deg)	C1-N1 Bond Length (A)	Total Potential Energy (kcal/mol)	Activation Barrier (kcal/mol)	Notes on Generation
Anti	PM3	156.9	2.111	-18043	0.31	- Placed N1 at 1.6 A off C1 - MM Optimization for fixed EO molecule - PM3 Optimization for 6 cycles - Eigenvector transition state search
Anti	AM1	156.9	2.199	-19890	-0.31	
Anti	RM1	154.5	2.13	-19798	-5.42	
Anti	Ab Initio *-Geometry by RHF-6-31G** *- Energy calculated by RHF-6-31G**	164.3	2.291	-130744	-6.5	- PM3 transition state optimization - Eigenvector transition state search
Anti	Ab Initio *- Energy calculated by MP2/RHF-6-31G**			-131144	-17.4	

To understand how these errors materialize across the reaction surface, the following procedure was used to map the IRC:

1. A restraint was placed on the C-N formed bond utilizing an artificial force constant on the bond length. The magnitude of this restraint was varied between successive runs.
2. The ammonia anion was placed close to its position in the transition state on the reactant side.
3. A geometry optimization was run to full convergence utilizing various methods (PM3, AM1, RM1, RHF-6-31G*).

The benefit of this procedure is the reaction coordinate may be manipulated such that individual points along the pathway become stable due to the impact of energy from the C-N bond restraint. The energy introduced to the system as a result of this restraint is given by the following equation.

$$E_{Pot} = k(l_{res} - l_{actual})^2 \qquad (2.1)$$

where k is in kcal/mol/A^2

As the magnitude of the force constant is increased, the total system has a greater potential to cross energy barriers. (8) This is the mechanism used to cross the transition state and is evident in the energy profile when the IRC is plotted against the C-N bond length. To be of use quantitatively for prediction of the energy barrier, a correction must be made per the equation above to account for the potential energy added into the system by the restraint.

Figure 2-7 shows the difference seen between three various calculation methods. The PM3 profile shows a large amount of discontinuity compared to either the *ab initio* method or MNDO method. This discontinuity occurs at two locations. The first is associated with a large energy benefit achieved due to the docking of the anion off one of the hydrogens on the EO molecule. The largest energy benefit occurs when the anion lies in the same line as the C-H bond. Once the bond is restrained such that large core-core repulsion exists between the hydrogen and amine anion, the angle of attack rotates out of this plane and the energy benefit disappears. The MNDO model does not show this benefit. This is not surprising given AM1 and subsequently PM3 were parameterized to address insufficiency of the MNDO to accurately predict the effects of hydrogen bonding. The *ab initio* method employed clearly showed the effects of orbital overlap as the anion came in close contact with EO and resulted in a smooth curve rather than the selection of mechanism of parameterized energy benefits that dominates the PM3 method.

Of further interest is the jump in energy predicted by PM3 in the vicinity of the transition state. This same phenomenon was noted during benchmarking studies performed on a methyl amine – propylene oxide reacting system. The transition state structure predicted by PM3 falls directly in the region depicted by the two elevated points in Figure 2-7. It is not clear exactly what parameters within the PM3 regression drive this phenomenon, but is likely the driving force behind the systematic over-estimation of transition state energies noted in literature and summarized above. Therefore, based on these observations, the PM3 is not qualified to perform quantitative and accurate predictions of reaction coordinate modeling for the EO-NH2 system. It is likely the use of this method will overestimate the benefit of a hydrogen abstraction compared to experimental reality.

Figure 2-7. IRC under a Restrained C-N Bond Length for EO-NH2 System

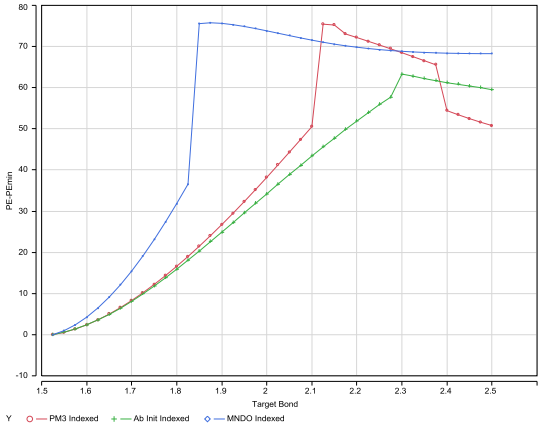

Chapter 3. Potential Energy Surface of Nucleophile / Epoxide Nucleophage Interaction

System Description and Calculation Method

The epoxide nucleophage evaluated here is ethylene oxide. The molecule has been oriented such that the oxide ring lies in the Y-Z plane with the C1-C2 bond aligned with the Z-axis. The molecular orbital calculations of ethylene oxide were fully optimized utilizing PM3 and P-R gradient optimization. The resulting atomic coordinates are located in Table 3-1 with graphical depiction in Figure 3-2.

The potential energy surface estimated is done so with orbital mixing excluded during structure optimization. The atoms of the nucleophage, EO, were fixed in Cartesian space with the bonding atom of the nucleophile moved successively to generate a 3D grid. At each grid point, a MM geometry optimization was carried out on the system with C1 and N1 fixed in Cartesian space using HyperChem™ (3) running AMBER3. Once an optimum was found, the PM3 level potential energy was calculated and reported. Computational cost was reduced by simulating only one quadrant of the C2V symmetry. In each run, 20,000 points were generated in this manner using an iterative approach programmed in VBA for EXCEL™ to interact with HyperChem™.

Table 3-1. IRC under a Restrained C-N Bond Length for EO-NH2 System

	X	Y	Z
C1	0.000	-0.185	0.900
C2	0.000	-0.185	-0.583
O1	0.000	1.040	0.158
H1	-0.907	-0.405	1.476
H2	0.907	-0.405	1.476
H3	-0.907	-0.405	-1.159
H4	0.907	-0.405	-1.159

Figure 3-2. Illustration of EO/amine reacting system

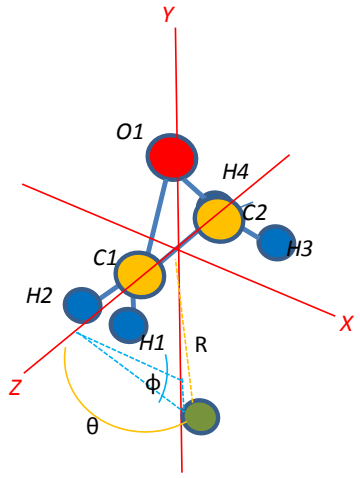

Results and Discussion

The purpose of this procedure is to probe the system for potential of bimolecular reaction. Qualitatively, the surface helps to illustrate the amount of energy required to elevate the reacting system along the intrinsic reaction coordinate (IRC) *before* any optimization takes place via molecular orbital mixing. By statistical mechanics, the probability of finding the system in any given state at equilibrium along this energy surface could be approximated utilizing the partition function shown below.

$$p_{PE}(i) = \frac{n_i e^{-E_i/k_B T}}{\sum_i n_i e^{-E_i/k_B T}} \qquad (3.1)$$

where n is the degeneracy of any given state i
k_B is Boltzmann's constant

The interactions between ethylene oxide and ammonia, the amine anion, and a hydrogen anion are shown in Figures 3-3, 3-4, and 3-5 respectively. While these figures and calculations don't provide significant insight quantitatively, they do help to form a picture of how the reacting species begin to interact with each other. Along the left side of each 3-D graph lies the C-O-C plane.

In the first, Figure 3-3, the oxygen and leading carbon in the ring are discernable as red spheres because of the increase in energy required for the nucleophile to occupy space in close proximity to these atoms. The energy profile across the surface is fairly uniform.

Figure 3-3. Potential Energy of NH3 Interaction with EO

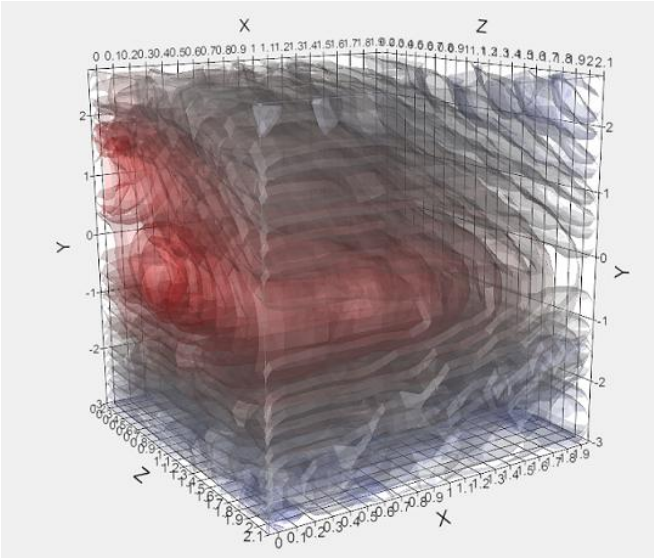

Figure 3-4. Potential Energy of Amine Anion Interaction with EO

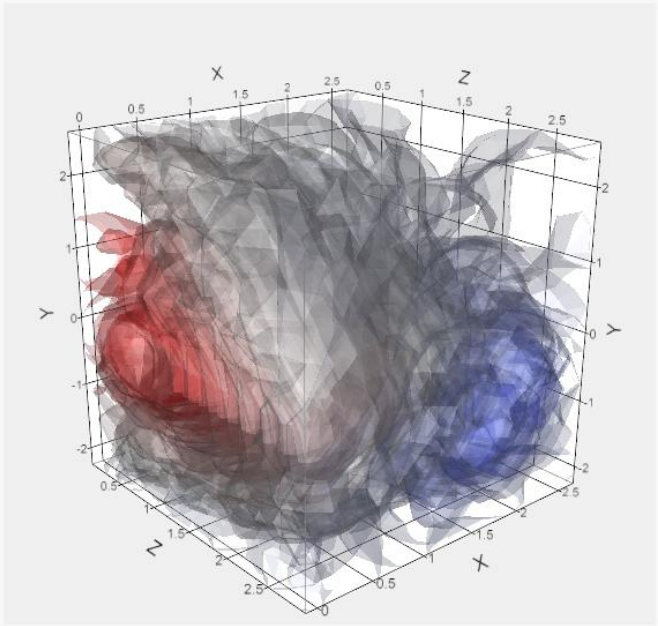

Figure 3-5. Potential Energy of H Anion Interaction with EO

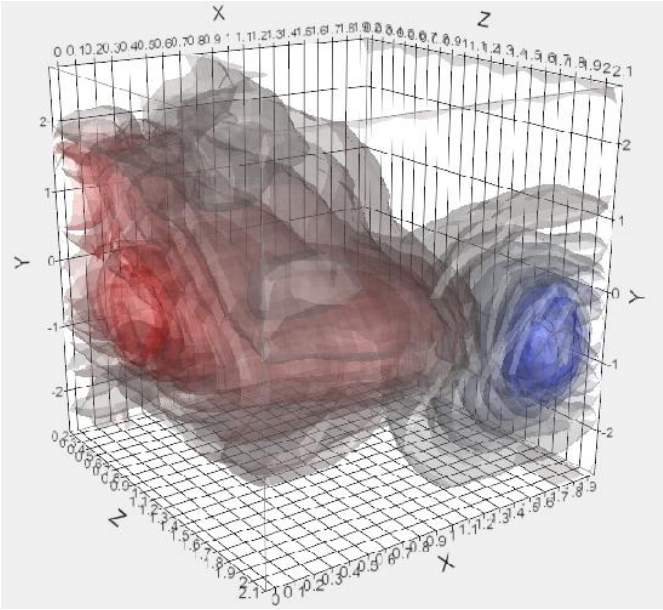

However, large regions of low energy volume exist in Figure 3-4 and 3-5. In Chapter 2, the energy benefit from hydrogen-lone pair bonding calculated was noted. Here this effect becomes visually evident. With successive runs of increasing nucleophillic strength, a low energy well develops approximately 1 A from the oxirane hydrogen where the nucleophile lies in-line with the C-H bond.

The impact of inaccurate PM3 parameterization on a statistical model of reaction rate is significant. The probability of finding the nucleophile within the energy well dominates the interaction. For the EO-NH2 reacting

system, 98.5% of the total partition function may be explained by 0.005% of the sampled points all located within this well. The resulting probability is depicted in Figure 3-6.

Figure 3-6. Probability of locating the amine anion in Cartesian space

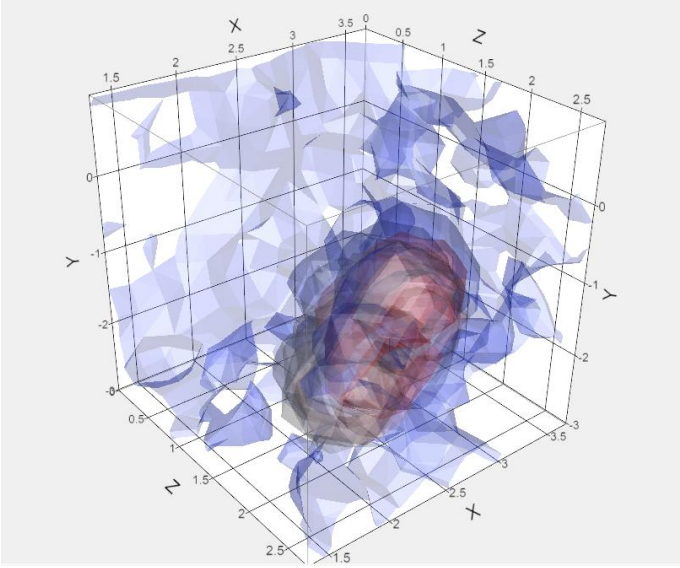

Chapter 4. Generation of the EO-NH3 Probability of Reaction and Transition Surface by Monte Carlo Simulation

Introduction

The concepts used to generate the potential energy surface are expanded in this section to include a subsequent optimization utilizing Monte Carlo sampling. Once an optimized geometry is found using MM methods, the complex is allowed to move as a function of probabilities derived from the Boltzmann distribution (3.1) for a given temperature. The enabling energy for the move is calculated by PM3 level of theory and selected randomly as a sample from the probability distribution. Sufficient steps are run to allow the complex to come to equilibrium where both the structure and energy are stable.

It is possible through implementation of Monte Carlo sampling to estimate bulk and thermodynamic properties of a given system as a function of temperature. It is important during the estimation of these properties that sufficient time is given for the system to come to equilibrium. This is typically monitored by calculation and stability evaluation of the energy derivative as a function of d(step). (8) Stability for this purpose (i.e. number of runs) could be defined by statistical means; however, a simple approach of 100 steps based on observation of the reacting system was implemented.

Background

At this point, it is necessary to describe the process to transform the data collected during a Monte Carlo simulation of epoxide ring opening reaction to reaction rate constant. The history of statistical reaction rate modeling is summarized well in several works (9) (10) (11) and is recounted in Figure 4-1. There have been multiple paths taken subsequent to these works to address underlying issues with the methodology. Of interest is semiclassical transition state theory (SCTST). The method combines quantum mechanical scattering with transition state theory, although avoids the presumption of separability of motion along a reaction coordinate (12) (13). This means that the partition function for the activated complex does not need to be separated to enable the incorporation of the negative vibrational frequency required to implement TST. SCTST begins with the same concepts that are present in RRKM.

The fundamental equation behind the RRKM method is the microcanonical rate constant as given by equation 4.1.

$$k(E) = \frac{1}{h}\frac{G(E)}{\rho(E)} \tag{4.1}$$

Where h is Plank's constant, G(E) is the Cumulative Reaction Probability (CRP), and ρ(E) is the density of states. The thermal rate constant, k(T), may be derived from this equation by integrating across k(E) using the Boltzmann's distribution resulting in Eq 4.2.

$$k(T) = (h\emptyset_A)^{-1}\int_{E_0}^{\infty} G(E)\exp\left(\frac{-E}{kT}\right)dE \tag{4.2}$$

In this expression, $\emptyset_A$ is the volume specific partition function of the reactant. The above equations are formally correct. With full and precise integration of the above variables across all quantum mechanical states as is attempted in quantum scattering techniques, no further assumptions or corrections are necessary. The benefit of the method is it provides a means to estimate flux across the dividing surface between reactant and product without requiring separation of coupling across degrees of freedom. The computational cost for full

Figure 4-1. Monograph depicting evolution of statistical rate constant prediction methods

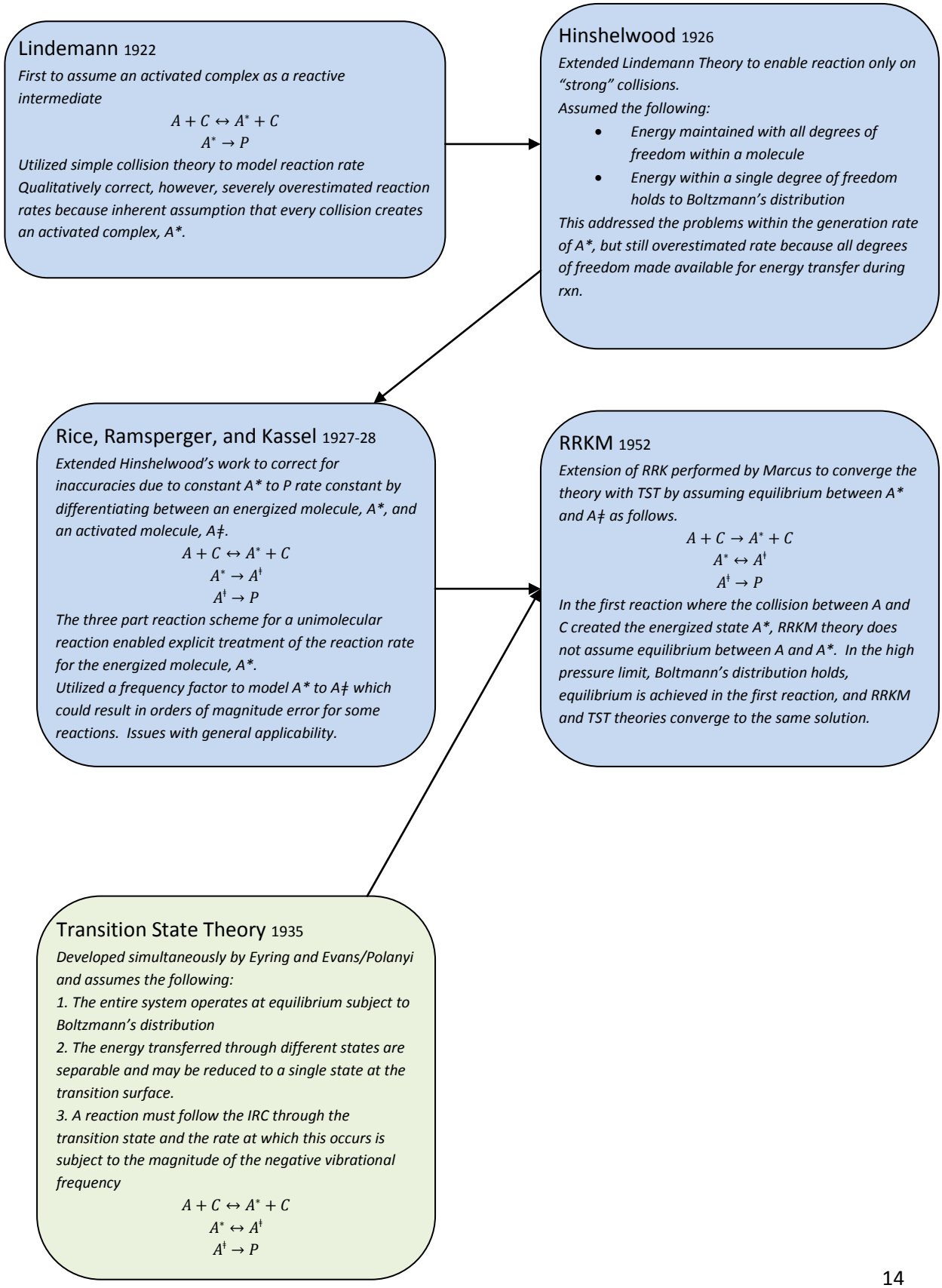

implementation is of course prohibitive, although for very small systems, 3-4 atoms, this has been attempted with good results.

Derivation of Method

The reaction scheme presented in this work is depicted below. The difference between this methodology and those presented in Figure 4-1 aside from being a bimolecular reaction, is that the premise is not constrained by assumptions of equilibrium. A full implementation, which will not be performed here, could easily be manipulated to drive the reverse of each of these reactions. In this manner, it is very similar to SCTST, although would use a different mechanism to estimate the second reaction to yield the activated complex from the energized complex.

$$E + A \rightarrow EA^*$$
$$EA^* \rightarrow EA^{\ddagger}$$
$$EA^{\ddagger} \rightarrow P$$

Practically, the data used to illustrate the methodology was taken from low pressure gas phase EO/NH2 reaction (14). Clearly this does not prove out the method, but does allow for illustration of key parts of this study. Because the first reaction at low pressures will be rate controlling, the system may be defined as:

$$E + A \rightarrow EA^* \quad (1)$$
$$EA^* \leftrightarrow P \quad (2)$$

and the fundamental equation used to derive reaction rate is therefore:

$$r_i = \int p_{PE} p_{rxn} p_i dPE * \frac{\delta(Reacting\ Group\ Collisions)}{\delta t} \tag{4.3}$$

In the above equation, r_i is the rate of reaction to yield intermediate or product complex *i,* p_{PE} is the probability that a system with a known average kinetic energy will achieve a given coordinate on the potential energy surface, p_{rxn} is the probability that any reaction will take place for a given coordinate on the potential energy surface, and p_i is the probability that if a reaction takes place it will be a reaction to yield species *i.*

For the moment, the exact definition of EA* relative to E and A will not be defined. The transition of E and A to EA* will take place as a function of frequency of interaction while probability of reaction will be managed through the transition of EA* to P. This approach is holds similarities across several of the methods presented in Fig 4.1, especially that of the "strong" collision frequency forming the basis of Hinshelwood theory.

For an ideal gas, which for this work will be assumed here forth, this frequency for the first reaction may be expressed in terms of binary collision theory, however, statistical sampling from a molecular dynamics simulation may be used to express this frequency as well. The intent is that increasingly complex systems may be expressed utilizing an interaction frequency without requiring significant computational resources to understand all potential transition states. The second reaction may therefore be expressed in terms of reaction probability as a function of the internal energy of the system relative to the barrier height. This reaction is assumed to be very fast relative to the collision frequency and for convenience, where EA* exists in equilibrium with P. The equilibrium assumption between EA* and P enable the overall reaction probability is embedded in the equilibrium constant, although in reality, no equilibrium exists.

Now EA* must be defined. The boundary of EA* is the radius between the two molecules where E begins to interact with A and exists as an optimum between the frequency expression and the equilibrium expression.

Stated rigorously, the physical boundary of what we define as EA* is drawn where the frequency expression may be dominated by the volume specific translational partition function for the system outside of EA* while the equilibrium expression may be dominated significant by the internal energy partition function for the system inside of EA*. The latter reduces to a unimolecular reaction that may be treated by RRKM theory through Eq. 4.1. (15) Following the derivation presented by Khundkar, Marcus, and Zewall (16) through combination of Eq. 4.1 and 4.2, the rate constant is given by

$$k(T) = \frac{k_B T}{h} \frac{\emptyset^{\ddagger}}{\emptyset} e^{-E_0/k_B T} \tag{4.4}$$

where $\emptyset^{\ddagger}$ and $\emptyset$ are the volume specific partition functions of the transition state and the reactant respectively. The overall partition functions are given by the product of the individual partition functions. For convenience, the vibrational, rotational, and electronic partition functions are wrapped into an internal partition function per Eq 4.6.

$$\emptyset = \frac{Z_{A,tr}}{V} Z_{A,vib} Z_{A,rot} Z_{A,el} \tag{4.5}$$

$$Z_{A,int} = Z_{A,vib} Z_{A,rot} Z_{A,el} \tag{4.6}$$

Combining equations 4.4, 4.5, and 4.6 yields the following:

$$k(T) = \left(\frac{k_B T}{h}\right) \left(\frac{\emptyset_{tr}^{\ddagger}}{\emptyset_{tr}}\right) \left(\frac{Z_{int}^{\ddagger}}{Z_{int}}\right) e^{-E_0/k_B T} \tag{4.7}$$

The translational partition function is described by Eq. 4.8 and is a constant for a given mass of EA*.

$$\emptyset_{tr} = \left(\frac{2\pi m_{EA} kT}{h^2}\right)^{3/2} \tag{4.8}$$

Because the interacting system between E and A are considered a unimolecular system, the ratio of the translational partition functions of transition state and reactant is equal to unity.

To see the impact of the decision boundary of EA*, a simplified model for the rotational and vibrational partition functions is all that is needed. First, the impact of the chosen EA* boundary on the rotational partition function is determined. The characteristic rotational temperature is given by:

$$\theta_r = \frac{h^2}{8\pi^2 k_B I_E} \tag{4.9}$$

Where I_E is the moment of inertia for the rigid rotor with ends of E and A. The moment of inertia is calculated by Eq 4.10.

$$I_E = \mu r^2 \tag{4.10}$$

Where μ is the reduced mass. Therefore, the characteristic temperature is inversely proportional to the square of the radius of interaction. For conditions where θ_r<<T, the rotational partition function may be approximated by Eq 4.11.

$$Z_r = {}^{T}/_{\theta_r} \tag{4.11}$$

Therefore, $Z_r \propto r^2$. The conceptual explanation is rooted in the theory behind RRKM. For isomerizations or molecular rearrangements in unimolecular systems, the energy flow through the molecule is constrained from a

large number of states to a minimum at the transition state where the molecule must tunnel to the alternate configuration. The result is an increasingly negative change in entropy as the transition state is approached. If the beginning configuration is given an increasingly large number of quantum rotational states due to large radius of interaction that will become the formed E-A bond, the probability that the molecule will funnel energy to the constrained transition state will decrease and therefore the rate constant will become lower.

From binary collision theory of hard spheres, the following equation describes the number of collisions / unit volume / time.

$$Z_{AB} = 2n_a n_b {\sigma_{AB}}^2 \left(\frac{2\pi kT}{\mu}\right)^{1/2} \tag{4.12}$$

where n_a and n_b are the number of particles / volume of species A and B, σ_{AB} is the radius of separation between the two species, and μ is the reduced mass. It can be seen from this expression, that the collision frequency is proportional to the square of the radius of interaction. If only rotational and translational partition functions are considered, the two offset for all space and the choice for the radius is arbitrary.

The complication comes with the inclusion of the vibrational partition function which is given by Eq 4.12.

$$Z_{vib} = \prod_{n=1}^{m} \frac{1}{1-e^{-\theta_{vi}/T}} \tag{4.13}$$

where m is the number of vibrational modes given by 3N-6 for a nonlinear polyatomic molecule, θ_{vi} is the characteristic temperature of the vibrational mode and is given by Eq 4.13.

$$\theta_{vi} = \frac{hc}{k}\omega_{ei} \tag{4.14}$$

The implications of inclusion of the vibrational partition function can be imagined by a reverse path from the TS to isolated reactants. There will be 6 additional vibrational modes associated with the transition state that will disappear to 0 s^{-1} frequency in the case of an infinite length of the formed bond. The inclusion of this mode in the vibrational transition state forces the corresponding unimolecular vibrational partition function also to infinity. The choice of the radius of interaction between E and A, σ_{AB}, will therefore be important with regard to the vibrational partition function, but not with regard to the combination of the translational and rotational partition functions.

To address this complication, a rearrangement of Eq. 4.1 will be performed. Conceptually, the following will occur for a reaction to proceed forward:

1. The transition surface will be defined as that surface of interaction between the reacting species where there exists a 50% probability of reaction. An example taken from the EO/NH3 system is located in Figure 4-2 where the red dots represent a location where a reaction occurred during a Monte Carlo simulation and the size of the marker indicates the relative probability of reaction.

2. The transition surface will exist orthogonal to the IRC and will reach a minimum energy where the IRC crosses the transition surface. This is very similar to the so named hypersurface present throughout much of reaction theory.

3. The interaction radius, σ_{AB}, will be set to the maximum distance between the reacting species along the transition surface. Because the δl_{AB} is likely to be very small compared to the interacting velocity of the two molecules, the difference will be neglected. The implication is that $\emptyset^{\ddagger} = \emptyset$ and therefore $\frac{\emptyset^{\ddagger}}{\emptyset} = 1$.

Figure 4-2. EO/NH3 Transition Surface weighted by probability of reaction

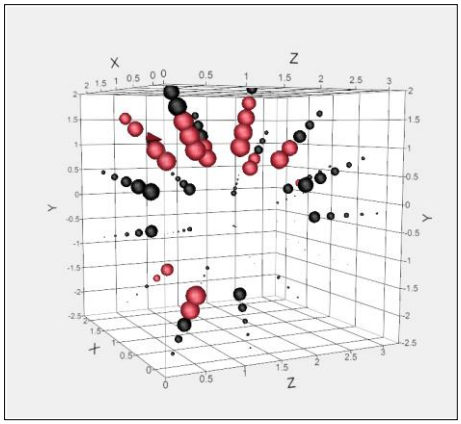

4. The rate constant for reaction of the unimolecular complex is therefore:

$$k_2(T) = \frac{k_B T}{h} \int_0^{2\pi} \int_0^{\pi} \gamma(\theta, \varphi) e^{-\dot{E}_0(\theta,\varphi)/k_B T} d\theta d\varphi \qquad (4.15)$$

where $\dot{E}_0(\theta, \varphi)$ is the area specific energy barrier to achieve the location along the transition surface and $\gamma(\theta, \varphi)$ is a step function that is equal to 1 when the combination of θ and φ lie within the transition surface and equal to 0 otherwise.

5. The rate constant for creation of the unimolecular complex is therefore:

$$k_1(T) = 2N_A {\sigma_{AB}}^2 \left(\frac{2\pi kT}{\mu}\right)^{1/2} \left(\frac{A_{TS}}{4\pi {\sigma_{AB}}^2}\right) \qquad (4.16)$$

where A_{TS} is the area of the transition surface. This far right term was included to account for the restricted area corresponding to the identified reaction path.

Chapter 5. Determination of Meta-Stable and Stable Complexes Formed During Bimolecular Interaction

Background

It is necessary in the course of this exercise to determine potential products or stable intermediates that represent minima on the potential energy surface. While any basic evaluation of the system would naturally predict a ring-opening reaction between the epoxide and nucleophile yielding a zwitterion intermediate, the effort to estimate the rate constant of this reaction by probabilistic methods is complicated by the following:

1. ***The assumption that every path across the transition surface yields the same species is not valid***
   The dominating reaction in ring opening kinetics proceeds by Sn2 mechanism. If we are able to calculate the probability that any reaction occurs, we clearly cannot assume that the species formed are path-independent. This may seem at first a trivial statement. Using traditional TS search algorithms, once a TS is identified, the "product" or species formed during traverse across the TS is easily identified by following the energy gradient until a minima is reached. Therefore, if the rate to open an epoxy ring is desired, one must simply identify the transition states that lead to this product or intermediate. When utilizing a probabilistic transition surface, TS structures are not found. Therefore, some method must exist to correlate any given coordinate along the transition surface to a subsequent product or intermediate species formed.

2. ***The final rate constant calculated is path dependent***
   In all but the simplest systems, the path from reactant to product occurs by movement through successive minima. The rate constant is equal to that of the rate limiting step or that of the highest relative energy barrier between minima. In the limiting case where the IRC is one-dimensional, only one TS exists between successive local minima or intermediates along the path from reactant to product.

   If two transition states exist to the same product, the reactant may travel via either path involving intermediates that are stereoisomers of each other. As these isomers are formed along each path, environmental influences on the rate of successive movement between intermediates may alter the preferred path. The relative barrier heights of anti and syn amination of ethylene oxide, for example, is indicated below in Figure 5-1. (2) The anti conformation, or underside ring attack, is the preferred path to form the aminated zwitterion complex. However, in the absence of an external proton source, only the syn conformation, or topside ring attack, is capable of forming the final product by proton transfer from the amine functional group to the oxygen.

Figure 5-1. Intrinsic Reaction Coordinate for EO-NH3 system

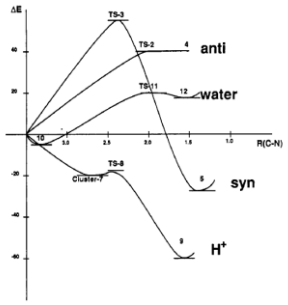

While this concept is elementary for a discrete number of transition states, it is a critical distinction in this work. The model to identify potential species formed during reaction must take into account enough information to distinguish between atomically identical complexes of varying configuration.

3. ***The distinction between reactant, product, and intermediate species is arbitrary***
   The primary issue to be resolved in this complication is to determine what is meant by species. The distinction even between reactant and product is an arbitrary one and is only made based on the barrier height relative to the resolution with which the energy surface was searched. As this resolution becomes tighter, every local minimum along a potential energy surface could be identified as an optimum structure for a distinct species along the IRC. The accuracy of the rate constant to form a given "product" species is therefore dependent on what group of structures is given the designation of "product".

To group structures into species, we must first identify the most probable conformations. This may be achieved by utilizing the data from the previous Monte Carlo simulation of the potential energy surface within a K-means clustering algorithm. During the generation of this data, critical bond lengths and angles were logged for each Monte Carlo step, *M,* and each seed structure, *N,* yielding *MN* potential structures to include in this process. To maximize the effectiveness of any clustering method, the first *M'* Monte Carlo species were culled from the data set to exclude high transient species from consideration. It should be noted, there are three parameters now influencing the complex search: *N, M, and M'.* Therefore, this is not an unsupervised search, but rather the three parameters much be chosen to optimize number of data points to accurately estimate the general population, (*N-M')*M*, the likelihood of following all probable reaction coordinates across the transition surface, *N,* the likelihood of reaching an equilibrium structure, MN^{γ} where γ is the Monte Carlo step size, and computational cost (*NM)*.

This exercise yields a series of structures that may be considered meta-stable or stable intermediates along the potential energy surface. This is particularly useful as a qualitative evaluation of any reacting system because no prior knowledge is required to generate potential reaction paths. The procedure, outlined below, is fairly robust to reasonable changes in the parameters *N, M, and M'*. As shown below, the procedure may also be used directly to estimate barrier heights for reaction, however, the surface would need to be explored at a resolution of several orders of magnitude higher to predict barrier heights with random placement along the surface. All statistical calculations performed were done so with JMP™.

Procedure to Generate Semi-Stable or Stable Complexes

1. *Generate Monte Carlo PES utilizing constant ray method as described above while logging critical bond lengths and angles*

   N = 150 *(Seed structures optimized utilizing MM methods)*
   M =100 *(Number of Monte Carlo steps implemented per structure)*

2. *Choose M' to limit data set to a semi-equilibrated state*

   Statistical methods could be used to optimize between number of points available for calculation vs. stability of the system, however, for this exercise, the number of Monte Carlo steps to pseudo equilibrium was identified by inspecting the epoxide ring bond angle vs. step number shown below. The points highlighted in red and modeled by spline fit were those containing a significant number of points that were identified as outliers vs. the normal distribution of the ring angle across the entire population. The system was assumed to reach pseudo equilibrium by step 63.

   M'=63

   Figure 5-2. Monte Carlo trajectories by reactant configuration seed

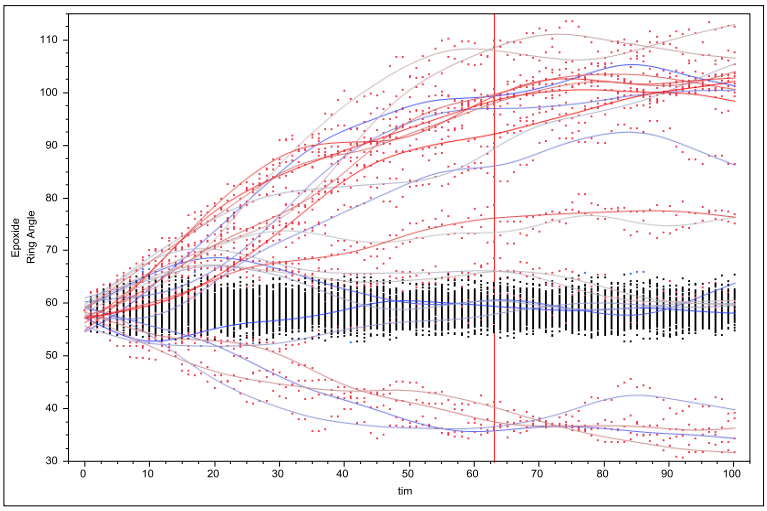

3. *Determine number of optimum clusters for a path independent reaction coordinate*

   A hierarchical clustering method was completed versus all identified critical bond lengths and angles using Ward's minimum variance method. This method generates a distance between each successive cluster, *D*.

$$D_{kj} = \frac{\left\|\overline{X_k} - \overline{X_j}\right\|^2}{\frac{1}{N_k} + \frac{1}{N_j}}$$

   The optimum number of clusters corresponds to the minimum number required to explain the majority of the variance across the dataset. This is certainly a subjective decision. However, critical number of clusters may be identified where large changes occur in the summed distance across all clusters. To evaluate this, outliers in $d(\log(\sum_k \sum_j D_{kj}))/d(\#\ clusters)$ vs. # clusters were identified using jackknife distances. By analysis, the number of clusters to be used will be 6 (outlier in derivative at cluster 5).

Figure 5-3. Ward's Distance as a function of number of clusters

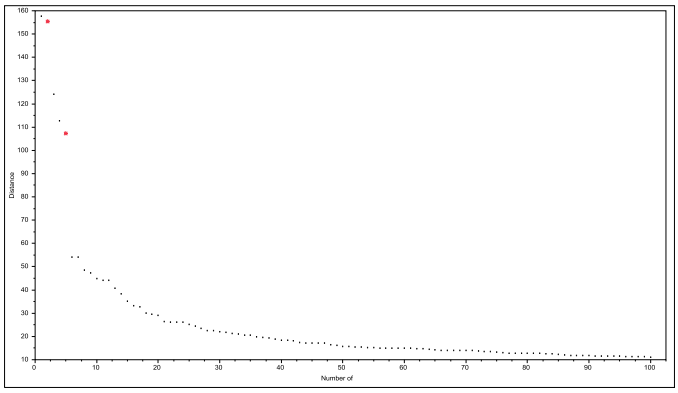

Figure 5-4. Jackknife plot identifying critical number of clusters by outlier analysis

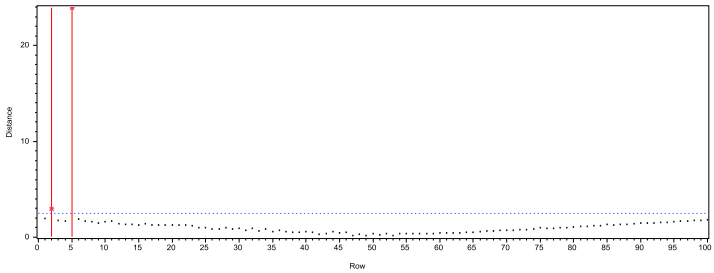

4. Utilize K-means clustering with optimal number of clusters to identify statistical significant complexes

A K-means cluster analysis is performed with the optimal numbers of clusters identified previously with Ward's minimum variance method. The additional clustering analysis is completed because of the useful information it provides with respect to mean structural configurations and the variance within each configuration identified as a stable or semi-stable complex. A biplot, the graph indicating each cluster vs. first and second principle components, of the result is provided below illustrating by color each of the clustered species for the NH3-EO reaction at 300 K.

Figure 5-5. Biplot of clustered NH3-EO complex species

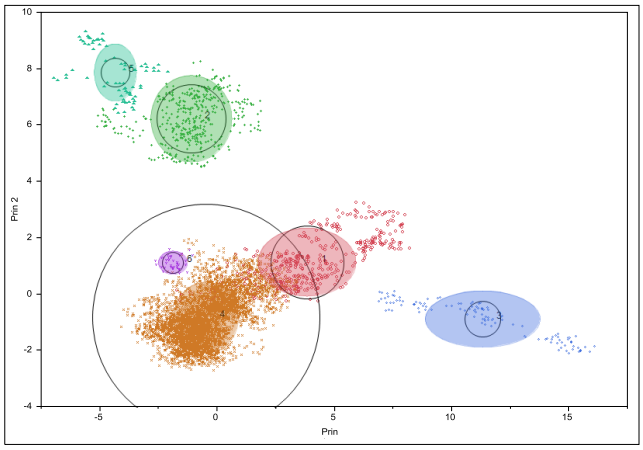

5. Summarize data from clustering

Table 5-6 contains averaged data for all tracked variables. Significant changes are highlighted in red for increases in value and green for decreases. In this analysis, cluster 4 corresponds to the unreacted species while cluster 2 corresponds to the product of the ring-opening reaction. Four other clusters were identified; however, the entry barrier depicted by the lowest potential energy value for a given cluster is ~30 kcal/mol higher than that of the ring opening reaction. Figure 5-7 shows the potential energy distribution by cluster.

Table 5-6. Critical variables in NH3-EO complex describing clustered species

	Cluster					
Variable	**1**	**2**	**3**	**4**	**5**	**6**
C1C2Bond	1.5	1.5	2.2	1.5	1.3	1.5
C1O1Bond	1.4	2.3	1.4	1.4	2.6	1.4
C1H1Bond	1.1	1.1	1.1	1.1	1.1	1.1
C1H2Bond	1.7	1.1	1.1	1.1	1.1	1.1
C1H3Bond	2.2	2.2	2.7	2.3	2.1	2.1
C1H4Bond	2.3	2.2	2.8	2.2	2.1	2.2
C1N1Bond	2.1	2.0	2.0	2.5	2.5	2.4
C2O1Bond	1.4	1.4	1.4	1.4	2.6	2.3
C2H1Bond	2.3	2.3	2.8	2.3	2.1	2.2
C2H2Bond	2.7	2.3	3.0	2.2	2.2	2.2
C2H3Bond	1.1	1.1	1.1	1.1	1.1	1.1
C2H4Bond	1.1	1.1	1.1	1.1	1.1	1.1
C2N1Bond	3.0	2.6	2.6	3.4	2.7	2.9
O1H1Bond	2.2	2.9	2.1	2.2	2.8	2.0
O1H2Bond	2.6	3.0	2.1	2.2	3.0	2.1
O1H3Bond	2.1	2.1	2.1	2.1	2.9	2.6
O1H4Bond	2.2	2.1	2.1	2.2	2.8	2.7
O1N1Bond	2.9	2.0	2.8	3.2	1.3	1.9
H1H2Bond	2.4	1.8	1.9	1.8	1.8	1.8
H1H3Bond	2.7	2.5	2.9	2.6	2.5	2.5
H1H4Bond	3.2	3.1	3.6	3.2	3.1	3.2
H1N1Bond	2.7	2.5	2.4	2.6	3.0	3.4
H2H3Bond	3.6	3.1	3.6	3.2	3.1	3.1
H2H4Bond	2.8	2.5	3.2	2.6	2.5	2.6
H2N1Bond	1.1	2.4	2.4	2.1	2.4	2.3
H3H4Bond	1.8	1.8	2.0	1.8	1.9	1.8
H3N1Bond	4.0	3.4	2.8	4.2	3.4	3.7
H4N1Bond	3.2	3.2	2.7	3.7	2.6	2.7
Epoxide Ring Angle	59	101	38	59	76	36

Table 5-7. Potential energy distribution by clustered NH3-EO complex

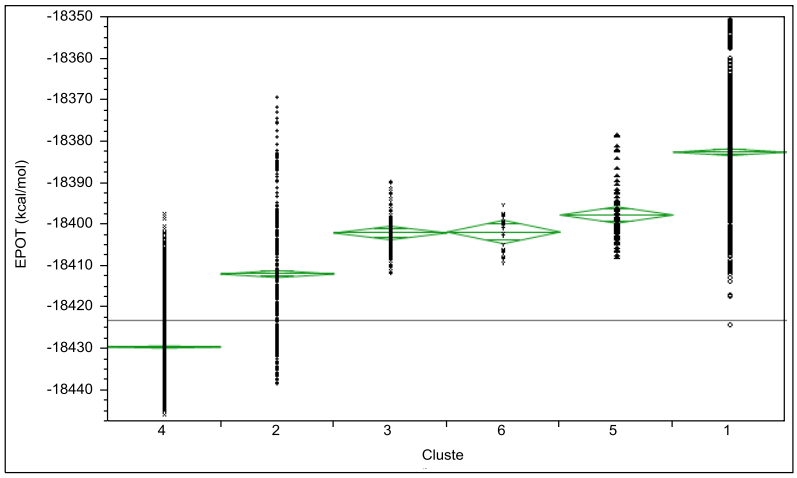

Chapter 6. Application to EO/NH2 Reacting System

Overview

Very little literature exists describing experimental rates of epoxide / amine systems in the gas phase. The EO/NH2 gas phase reaction rate was measured via afterglow method by Bierbaum et. al. (14) and will be used as a benchmark. While one data point is certainly not sufficient to understand the efficacy of the method presented here, it may be used as a qualitative comparison. The applicability of PM3 to the EO/NH2 reacting system was explored in section 2. There are key takeaways from this exercise. The PM3 level of theory will overestimate the probability of hydrogen abstraction from EO by the NH2 anion and will underestimate the reaction rate because of the step increase in energy across the transition structure.

Experimental Data

The data collected by Bierbaum et al (14) determined kinetic rate parameters at 300 K for the reactions of ethylene oxide and propylene oxide with three ionic species in the gas phase: OH^-, NH_2^-, and CH_3O^-. The rate constant for the ethylene oxide / NH_2^- reaction was determined to be 1.5E-10 cm^3/(particle*sec). Multiplying by 6.022E20 (particle*L)/(mol*cm^3) yields a rate constant in standard units of 9.03E10 L/(mol*s).

Utilizing binary collision theory, an estimate to the probability of reaction may be made. The number of collisions per unit volume per time is given by:

$$Z_{AB} = 2n_A n_B {\sigma_{AB}}^2 \left(\frac{2\pi kT}{\mu}\right)^{1/2} \tag{6.1}$$

Where n_A and n_B are the particle concentrations of A and B per cm^3 respectively, σ_{AB} is the mean hard sphere diameter of A and B, and μ is the reduced mass.

The pre-exponential factor given by kinetic theory from Eq 4.15 excluding the area term is therefore

$$A = 2N_A {\sigma_{AB}}^2 \left(\frac{2\pi kT}{\mu}\right)^{1/2} \tag{6.2}$$

For the ethylene oxide / NH_2^- system, μ is equal to 11.75 g/mol. Substituting in R for k (mol vs. particle), the right side of the equation for this system is equal to:

$$\left(\frac{2\pi RT}{\mu}\right)^{1/2} = \left(\frac{(6.283)\left(8.314\frac{J}{mol*K}\right)(300K)}{(11.75\ g/mol)(1kg/1000g)}\right)^{1/2} = 1.15E4\ dm/s \tag{6.3}$$

The pre-exponential factor in terms of the mean diameter in Angstroms is therefore equal to

$$\text{A}= \left[2 * (6.022E23\ particle/mol)\left(\frac{1dm^2}{1E18A^2}\right)(1.15E4\ dm/s)\right]{\sigma_{AB}}^2 \tag{6.4}$$

$$\text{A}= 1.39E10\frac{L}{mol*s}{\sigma_{AB}}^2 \tag{6.5}$$

The Arrhenius exponential factor, p_{rxn}, may therefore be solved for a given experimental rate constant.

$$\frac{6.52}{p_{rxn}} = {\sigma_{AB}}^2 \tag{6.6}$$

In Figure 6-1, the required probability of reaction to achieve the experimental rate constant (14) is graphed vs. the effective mean hard sphere diameter. For example, if the mean hard sphere diameter is ~2.5 A, 100% of collisions will on average result in a ring opening reaction.

Figure 6-1. Probability of Rxn Given Collision vs. Mean Hard Sphere Diameter

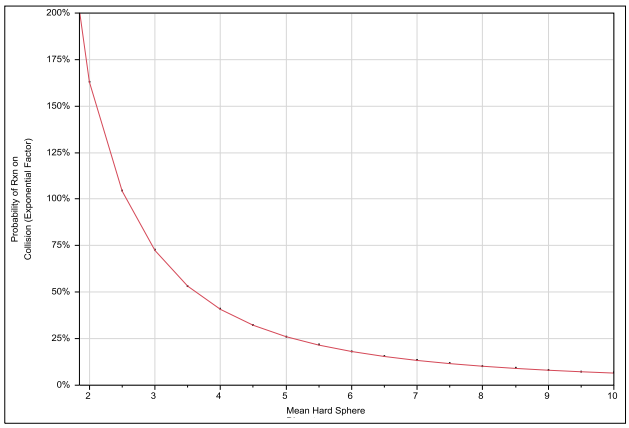

Determination of Stable and Meta-stable Complexes

A Monte Carlo simulation was run to explore the PE surface for reaction potential. In this case, 10 clusters were identified and used to model the data. The increase in number of statistically significant clusters compared to the EO/NH3 system presented in section 5 is likely caused by the reactivity of the NH2 anion nucleophile. Table 6-2 details each of the mean bond lengths relative to the length within the base cluster 2 along with the raw mean epoxide (O1-C2-C1) angle. There are two base clusters, 2 and 6, that represent a non-reaction. Cluster 6 represents the semi-stable complex created by docking the NH2 nucleophile off the ethylene oxide proton. The energy benefit of this was seen in the evaluation of PM3 in section 2 and is an anomaly of that semi-empirical method. Figure 6-3 shows the average and distribution potential energies (PM3) required to reach each cluster within the reacting system.

Table 6-2. Relative change from base cluster 2 for EO/NH2 System

	Cluster									
Variable	**1**	**2**	**3**	**4**	**5**	**6**	**7**	**8**	**9**	**10**
C1C2Bond	1.0	1.0	1.7	0.9	1.6	1.0	1.6	1.0	1.1	1.4
C1O1Bond	1.0	1.0	1.8	1.7	0.9	1.0	1.7	1.6	1.6	1.0
C1H1Bond	1.6	1.0	1.0	1.0	1.0	1.0	1.0	1.8	1.0	1.0
C1H2Bond	1.4	1.0	0.8	0.9	1.0	1.0	0.8	0.8	1.2	1.3
C1H3Bond	1.0	1.0	1.3	1.0	1.2	1.0	1.2	1.0	1.0	1.2
C1H4Bond	1.0	1.0	1.5	1.0	1.4	1.0	1.4	0.9	1.0	1.2
C1N1Bond	0.6	1.0	0.5	0.7	0.6	1.0	0.6	0.5	0.6	0.6
C2O1Bond	1.0	1.0	0.9	1.9	1.8	1.0	1.6	0.9	0.9	0.9
C2H1Bond	1.3	1.0	1.3	1.0	1.3	1.0	1.3	1.1	1.0	1.2
C2H2Bond	1.2	1.0	1.4	1.0	1.3	1.0	1.3	0.9	1.1	1.4
C2H3Bond	1.0	1.0	1.0	1.0	1.0	1.0	1.0	1.0	1.0	1.0
C2H4Bond	1.0	1.0	1.0	1.0	1.0	1.0	1.0	1.0	1.0	1.0
C2N1Bond	0.9	1.0	0.5	0.8	0.5	1.2	0.5	0.8	0.8	0.9
O1H1Bond	1.3	1.0	1.3	1.4	1.0	1.0	1.3	1.4	1.3	1.0
O1H2Bond	1.2	1.0	1.4	1.4	0.9	1.0	1.3	1.2	1.4	1.1
O1H3Bond	1.0	1.0	0.9	1.4	1.3	1.0	1.3	0.9	1.0	1.0
O1H4Bond	1.0	1.0	1.0	1.3	1.4	1.0	1.4	1.0	0.9	1.0
O1N1Bond	0.8	1.0	0.7	0.4	0.7	1.1	0.4	1.0	0.9	0.8
H1H2Bond	1.2	1.0	0.9	0.9	0.9	0.9	0.9	1.4	1.1	1.2
H1H3Bond	1.2	1.0	1.2	1.0	1.1	1.0	1.1	1.0	1.0	1.1
H1H4Bond	1.2	1.0	1.2	1.0	1.2	1.0	1.2	1.1	1.0	1.1
H1N1Bond	0.4	1.0	0.7	0.7	0.7	0.8	0.7	0.4	0.7	0.7
H2H3Bond	1.2	1.0	1.2	1.0	1.1	1.0	1.1	0.9	1.1	1.2
H2H4Bond	1.2	1.0	1.5	1.0	1.4	1.1	1.4	0.9	1.1	1.3
H2N1Bond	0.8	1.0	1.2	1.2	1.0	0.9	1.2	1.1	0.8	0.8
H3H4Bond	1.0	1.0	1.0	1.0	1.0	1.0	1.0	0.9	1.0	1.0
H3N1Bond	0.9	1.0	0.6	0.8	0.6	1.2	0.5	0.7	0.8	0.8
H4N1Bond	1.1	1.0	0.7	0.9	0.7	1.4	0.7	1.1	0.9	1.0
Epoxide Ring	*57.6*	*58.8*	*80.9*	*65.4*	*30.2*	*59.5*	*61.4*	*111.5*	*109.0*	*41.2*

Clusters 8, 1, 5, 3, 4, and 7 occur very infrequently and so are not considered likely reaction paths. Clusters 10 and 9 are significant in probability and are about equal in terms of average energy of the points leading to these clusters along the potential energy surface. Cluster 9 is the intermediate of the ring-opening reaction while cluster 10 is an intermediate formed when the epoxide ring is opened via the C-C bond. It is important to note that the average energy depicted in Figure 6-3 does not represent the energy barrier required for reaction to proceed forward for a real system, but rather is artificially increased for any given complex because there are points included where the two molecules were docked at extremely high energy points prior to initiating the Monte Carlo simulation. The cluster is simply the end statistical result of that Monte Carlo simulation.

Figure 6-3. Potential Energies for Each Clustered Product or Intermediate Complex

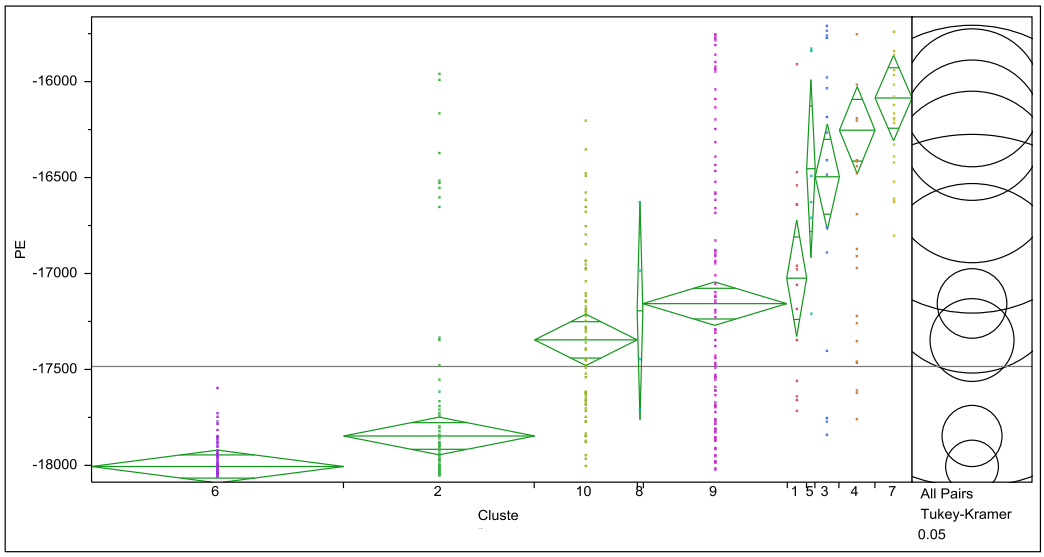

To determine if cluster 10 is a true potential intermediate, a series of repeated probability studies may be performed to determine where in Cartesian space the two clusters are most likely to overlap. That overlap is then explored to determine which complex is more likely to occur as two actual molecules approach each other. Figure 6-4 shows the most likely areas (i.e. cones) for a reaction to cluster 9 to occur. It can be seen from the figure there is an area of high probability within the anti region where phi is equal to $-\pi/2$. There is also an area of high probability within the syn region for values of phi > 0.5.

Figure 6-4. Areas of high probability for cluster 9 – Epoxide Ring Opening reaction

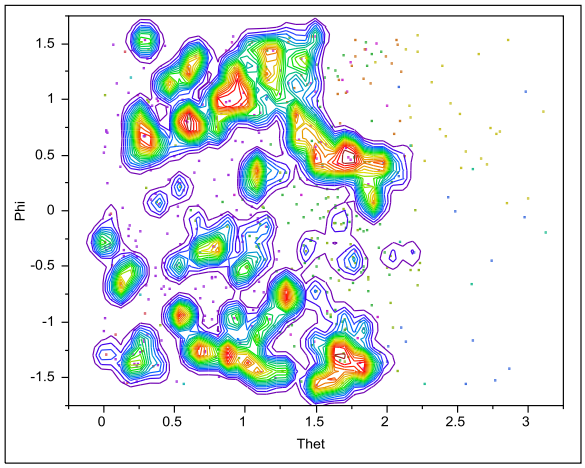

The areas of moderate probability or higher for both cluster 9 and cluster 10 were compiled into a single data table and the resulting cluster compared against R. As expected, cluster 10 does not become active until the nucleophile is < 1.5 A from the leading EO carbon atom. This is seen graphically in Figure 6-5. Cluster 9 becomes active around 2.1 A as expected from the transition state studies performed earlier. Beyond this region, no reaction takes place as only clusters 2 and 6 are present. Intuitively, this of course makes sense. One would not expect an epoxide ring opening reaction to occur via a C-C bond breakage.

Figure 6-5. Most probable cluster for overlapping 9/10 areas

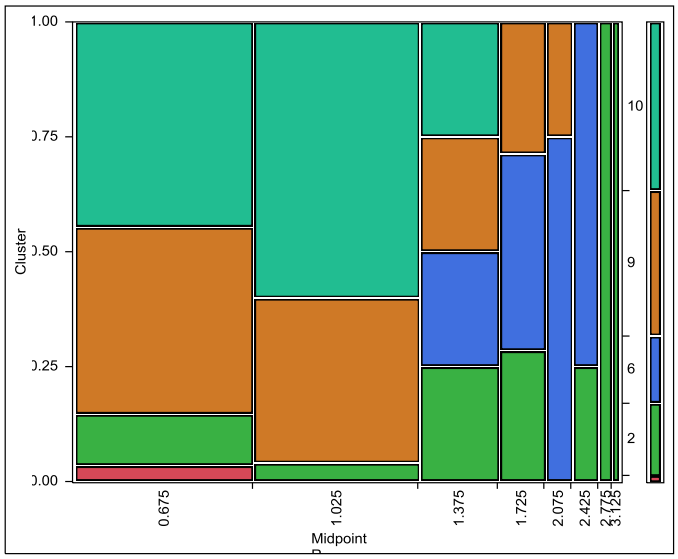

Determination of Reaction Probability

Now, the effective area available for reaction must be found. Figure 6-4 contains extremely valuable information relevant to this task. Another Monte Carlo simulation of much higher resolution will be performed in and around the areas where cluster 9 is most likely to result from the interaction. In the anti region of attack, phi is most concentrated around –π/2 to -0.6π/2. Figure 6-6 shows the 50% reaction probability surface for phi equal to –π/2. The red line represents the total potential energy of the reactants (-18043.12 kcal/mol). Therefore, for an anti attack of NH2 on EO, the reaction will be barrierless for theta values of ~1.15 - 1.7 radians. The red points are points where the Monte Carlo simulation resulted in reaction, the black represent points where the simulation did not yield a reaction. Of primary interest in this graph is that the minimum energy point lies at -18047 kcal/mol, 4 kcal/mol less than predicted by the transition state structure found by eigenvector search. The reason for this is not known, however, this is approximately the amount the PM3 method errantly increased by as the transition state structure was approached.

Within the graph depicting potential energy vs. R, the maximum R value that still meets the 50% reaction probability criteria lies just less than 2.2 A. This point represents the maximum distance from the leading carbon and therefore will be used within the estimate of the mean hard sphere diameter. This point, {0.01,-2.47,0.95}, lies 2.82 A from the center of mass of the ethylene oxide molecule and was the point where the nitrogen on the amine anion was located prior to running the Monte Carlo simulation. The distance between this point and the EO center of mass is equal to 2*(*mean radius)* and therefore is equal to the mean hard sphere diameter.

Figure 6-6. Monte Carlo potential energy surface for phi = –π/2

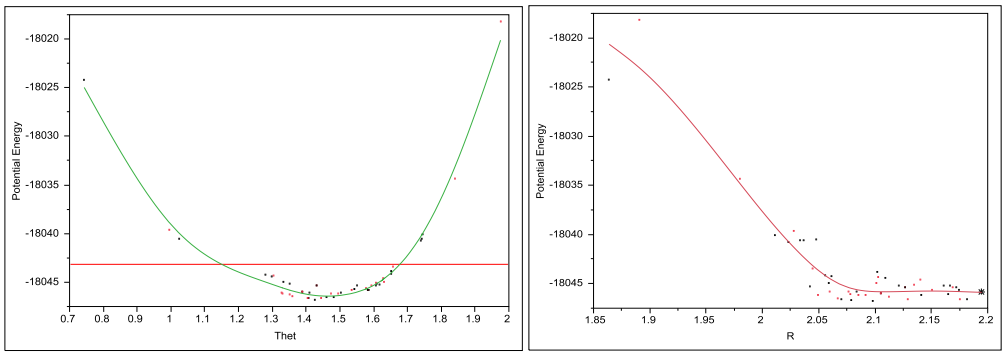

The simulation is repeated with phi = –0.8 π/2. Figure 6-7 shows the available area for reaction at this value of phi is much less compared to the positions at phi= -π/2 shown in Figure 6-6. Using the width of theta from these two simulations, the area within this quadrant available for the barrierless reaction is estimated to be 1.08 A^2. Because EO holds C2V symmetry, there are three other analogous regions to this area yielding a total area available for anti attack of 4.32 A^2. If average kinetic energy, 8.94 kcal/mol at 300K, was made available to traverse the energy barrier, the area available for anti attack would still only amount to ~ 13.5 A^2. With a total sphere volume of 99.9 A^2, the reaction probability on collision therefore is estimated at 4.3% for a barrierless reaction and 13.5% for an interaction of average kinetic energy at 300 K. This falls well short of the required 80% reaction probability predicted by Figure 6-1 for an interaction sphere of 2.8 A. Furthermore, it is unlikely that the syn configuration of attack participates in the reaction at this temperature due to repulsion between the anionic nucleophile and the negatively charged oxygen within the epoxide ring.

Figure 6-7. Monte Carlo potential energy surface for phi = –0.8 π/2

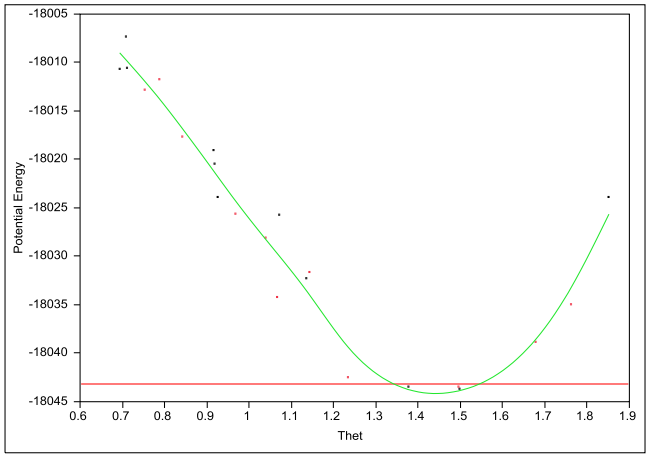

Chapter 7. Conclusions and Future Work

A method for reaction rate estimation was described in this work that has the potential to model complex systems without the paradigm decoupling of energy modes required by most conventional methods. If one hopes to apply a fundamental kinetic model to a macromolecular system, such as the epoxy curing reactions, the constraints placed on the method by a necessary decoupling of these modes must be overcome. The work presented attempted one possible avenue to address this issue, but also took steps to describe the simplest of ring opening reactions qualitatively.

Of particular interest was the ease of implementation of the clustering method to uncover potential intermediate and product species in a systematic and unsupervised manner as described in Chapter 5. At the conclusion of this clustering, one has all the necessary information at hand to speak meaningfully about potential reaction paths, even if the subsequent quantitative modeling fell short.

In addition, to gain potential insight into level of theory required to model the epoxy curing reactions, the semi-empirical method PM3 was evaluated for accuracy. While it performed very well for non-ionic reacting species, the method overestimated the attraction where the nucleophile was a charged species.

The reaction rate estimated utilizing the method with PM3 level of theory underestimated the reaction rate by a factor of 4. The most likely cause for the difference between the experimental and predicted reaction probabilities on collision is that channeling effects are not considered. To illustrate this concept, if the NH2 molecule approached the EO molecule with the phi value given in Figure 6-7 and a theta value of 0.9, the resulting potential energy of that location would be -18023 kcal/mol. This energy barrier is far higher than what is achievable by the system at 300K. The methodology used here assumes no reaction takes place at this point and moves on. In fact, if the two molecules approached each other at this angle, the most likely result is the high potential energy would simply divert the molecular complex into the well that exists at a theta of 1.45 and the reaction would proceed forward. The implementation as described here is not sophisticated enough to consider the probabilities that this would occur. In order to proceed forward and apply this general methodology quantitatively to more complicated systems, the data suggests additional work is required to strengthen the reaction / non-reaction probability barrier to account for translational, vibrational, and rotational channeling in reacting systems. This could be achieved either through implementation of a “shooting” method using a molecular dynamics simulation or by invoking an localized or “line-of-sight” equilibrium assumption to estimate reaction rate of the energized complex to yield the activated complex.

The work presented here and applied to the EO / NH2- reacting system, while lacking in quantitative accuracy for the final rate constant, provided the means to explore in detail all potential reaction paths without supervisory input, defined these paths and the resulting products via a statistical analysis, estimated the relevancy of each path through calculation of the average potential energy required to achieve the path, and confirmed through simulation the anti-configurational attack of ethylene oxide was most favored where the anion was used as the nucleophile. Ongoing work continues to improve on the methods presented and will attempt to close the deficiencies noted in the rate constant estimation.

Works Cited

1. **Petrie, Edward M.** *Epoxy Adhesive Formulations.* s.l. : The McGraw-Hill Companies, Inc., 2006. ISBN-10: 0-07-145544-2.

2. *Theoretical Study of the Reactions of Ethylene Oxide and Ammonia. A Model Study of the Epoxy Adhesive Curing Mechanism.* **Holubka, Joseph W, Bach, Robert D and Andres, Jose L.** 1992, Macromolecules, Vol. 25, pp. 1189-1192.

3. **Hypercube, Inc.** *HyperChem, Release 8.0.10 for Windows Molecular Modeling System.*

4. *Optimization of Parameters for Semiempirical Methods I. Method.* **Stewart, James P.** 2, s.l. : Journal of Computational Chemistry, 1989, Vol. 10, pp. 209-220.

5. *Reaction Kinetic Modeling from PM3 Transition State Calculations.* **Malwitz, Nelson.** 1995, Journal of Physical Chemistry, Vol. 99, pp. 5291-5298.

6. *Benchmark Calculations of Reaction Energies, Barrier Heights, and Transition-State Geometries for Hydrogen Abstraction from Methanol by a Hydrogen Atom.* **Pu, Jingzhi and Truhlar, Donald G.** 2005, Journal of Physical Chemistry A, Vol. 109, pp. 773-778.

7. Performance of PM6, PM3 and AM1 Methods. *MOLPAC2012.* [Online] http://openmopac.net/Downloads/PM6%20AM1%20PM3%20Main-Group%20raw%20data.xls.

8. **Hypercube, Inc.** *Hyperchem Release 8.* 2002. CC-109-110.

9. **Marcus, R A.** Theory, Experiment, and Reaction Rates. A Personal View. *J. Phys. Chem.* 1986, 90, pp. 3460-3465.

10. **Prentice, Boone.** Purdue Chemistry. *McLuckey Summer Lecture Series.* [Online] August 2011. [Cited: September 25, 2012.] http://www.google.com/url?sa=t&rct=j&q=mcluckeysummer%20lecture%20series&source=web&cd=1&cad=rja&ved=0CCIQFjAA&url=http%3A%2F%2Fwww.chem.purdue.edu%2Fmcluckey%2FGroupMeetingStuff%2F2011%2F2011%2520Summer%2520Lecture%2520Series%2F2011_Prentice_SL_RRKM.pdf.

11. **Fost, W.** *Theory of Unimolecular Reactions.* s.l. : Academic Press, 1973.

12. **Miller, W H.** Semiclassical limit of quantum mechanical transition state theory for nonseparable systems. *Journ. Chem. Phys.* 1975, Vol. 62, 5, pp. 1899-1906.

13. —. Semi-Classical Theory for Non-separable Systems. *Faraday Discussions Chem. Soc.* 1977, Vol. 62, p. 40.

14. **Bierbaum, Veronica M, et al.** Flowing Afterglow Studies of the Reactions of Hydroxide, Amide, and Methoxide Ions with Ethylene Oxide and Propylene Oxide. *Journ. of Am. Chem. Soc.* 1976, Vol. 98, 14, pp. 4229-4235.

15. **Miller, William H.** *Some New Approaches to Semiclassical and Quantum Transition State Theory.* s.l. : U.S. Department of Energy, 1990.

16. **Khundkar, L H, Marcus, R A and Zewall, A H.** Unimolecular Reactions at Low Energies and RRKM Behavior: Isomerization and Dissociation. *J. Phys. Chem.* 1983, Vol. 87, pp. 2473-2476.

17. *Ground States of Molecules. 38. The MNDO Method. Approximations and Parameters.* **Dewar, Michael J.S. and Thiel, Walter.** 15, 1977, Journal of the American Chemical Society, Vol. 99, pp. 4899-4907.

18. *Semiclassical transition state theory. A new perspective.* **Hernandez, Rigoberto and Miller, William.** 2, 1993, Chemical Physics Letters, Vol. 214, pp. 129-136.

19. *A practical implementation of semi-classical transition state theory for polyatomics.* **Nguyen, Thanh Lam, Stanton, John F. and Barker, John R.** 2010, Vol. 499, pp. 9-15.

20. *Semi-Classical Theory for Non-separable Systems.* **Chapman, S., Garrett, B.C. and Miller, W.H.** 1975, Journal of Chemical Physics, Vol. 63, pp. 2710-2716.